


## Wetting Phenomena: Line Tension and Gravitational Effect

Fei Wang (王飞)<sup>\*</sup> and Haodong Zhang

*Institute for Applied Materials - Microstructure Modelling and Simulation (IAM-MMS), Karlsruhe Institute of Technology (KIT), Strasse am Forum 7, 76131 Karlsruhe, Germany and Institute of Nanotechnology (INT), Karlsruhe Institute of Technology (KIT), Hermann-von-Helmholtz-Platz 1, 76344 Eggenstein-Leopoldshafen, Germany*

Britta Nestler

*Institute for Applied Materials - Microstructure Modelling and Simulation (IAM-MMS), Karlsruhe Institute of Technology (KIT), Strasse am Forum 7, 76131 Karlsruhe, Germany; Institute of Nanotechnology (INT), Karlsruhe Institute of Technology (KIT), Hermann-von-Helmholtz-Platz 1, 76344 Eggenstein-Leopoldshafen, Germany; and Institute of Digital Materials Science, Karlsruhe University of Applied Sciences, Moltkestrasse 30, 76133 Karlsruhe, Germany*

 (Received 24 January 2024; revised 5 August 2024; accepted 24 October 2024; published 11 December 2024)

An apparent contact angle is formed when a droplet is deposited on a solid substrate. Young's law has been employed to describe the equilibrium contact angle. Often in experiments, the equilibrium contact angle deviates from Young's law and depends on the volume of the droplet, known as the line tension effect. However, the physical origin of the line tension is quite controversial. Especially, the sign and the quantity of the line tension spanning 6 orders of magnitude are unsolved problems. Here, we quantify the line energy in terms of physical parameters and demonstrate that both positive and negative line tensions exist. The results are quantitatively compared with existing experiments as well as with previous theories.

DOI: [10.1103/PhysRevLett.133.246201](https://doi.org/10.1103/PhysRevLett.133.246201)

Wetting phenomena are broadly observed in our daily lives, such as dew on plant leaves [1,2]. The wetting effect is commonly described by an apparent contact angle at the triple junction of solid, liquid, and gas [3–5]. Hitherto, Thomas Young's theory [6] has been widely applied to describe the wetting effect and the equilibrium contact angle, known as Young's law. In this quintessential theory, the contact angle does not depend on the size of the droplet. However, decades of experiments show that the equilibrium contact angle often deviates from Young's law. Even contrary to Young's law, the experimental value of the equilibrium contact angle has a strong dependence on the size of the droplet, known as the line tension effect [7–9]. Yet, both the sign and the magnitude of the line tension are quite controversial. Specially, the line tension spans 6 orders of magnitude in literature [10]; no existing theories so far can fully address this fundamental problem.

The physical origin of the line tension is quite diverse in literature. Four main concepts are summarized as follows:

<sup>\*</sup>Contact author: fei.wang@kit.edu

*Published by the American Physical Society under the terms of the Creative Commons Attribution 4.0 International license. Further distribution of this work must maintain attribution to the author(s) and the published article's title, journal citation, and DOI.*

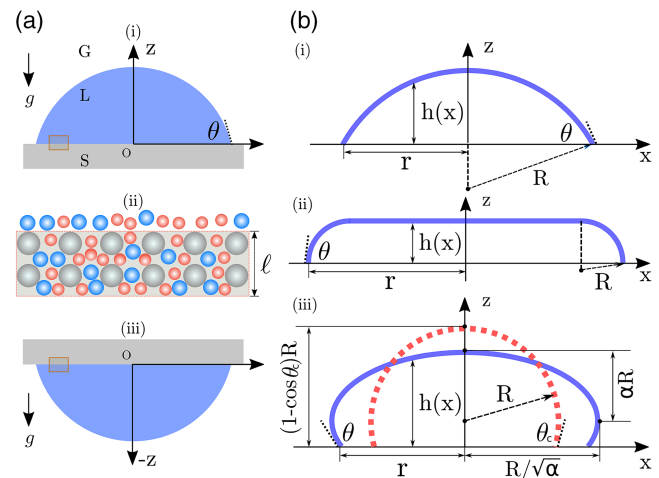


FIG. 1. (a)(i) Schematic sectional view for a sessile droplet on a solid surface.  $L$ , liquid;  $G$  gas;  $S$ , solid. (a)(ii) The penetration of the liquid (blue circle) and gas (red circle) species into the solid phase (gray) with a depth of  $\ell$ . (a)(iii) Sectional view for a pendant droplet. (b)(i) Bond number  $Bo \ll 1$ , where a spherical cap is formed. (b)(ii)  $Bo \gg 1$ , where a “pancake” droplet shape is established. (b)(iii)  $Bo \sim 1$ ; the droplet shape is approximated by an ellipsoidal cap with semiaxes of  $R/\sqrt{\alpha}$  and  $\alpha R$ . Here,  $R$  denotes the radius of an imaginary spherical cap (red dashed) with the same volume as the ellipsoid.

(A) Some researchers [11,12] argue that the line tension is an artifact of experimental error. (B) The second concept is the Tolman effect [13–15], where the surface tension of liquid–gas has a dependence on the size of the droplet. However, this leads to the puzzle for the sign and magnitude of the Tolman length [16]. (C) The density is nonuniform in the liquid [17]; especially near the solid surface, the density of the liquid is modified [3,18–21]. The variation of the density and the associated energy change the equilibrium contact angle. (D) Standard models [22–25] by adding a size-dependent line energy  $2\pi r\tau$  ( $r$ -base radius;  $\tau$ -line energy).

In this Letter, we consider the effect of the gravity on the wetting phenomena; for the first time, we derive the line energy in terms of physical parameters of the system. We show that the gravity effect can indeed lead to a line energy spanning from  $10^{-11}$  to  $10^{-6}$  N. We also demonstrate that both negative and positive line tension exist. The underlying mechanism for the transition between negative and positive line tensions is discussed.

We consider a droplet with the volume  $V = 4\pi R_0^3/3$  ( $R_0$  is an imaginary radius) on a solid surface, forming an apparent contact angle  $\theta$  and a base radius  $r$  (Fig. 1). The interfacial tension of liquid–gas, solid–liquid, and solid–gas is denoted by  $\sigma$ ,  $\gamma_{SL}$ , and  $\gamma_{SG}$ , respectively. We define the Bond number,  $\text{Bo} = \rho R_0^2 g / \sigma$ , to measure the ratio of gravity force to the surface tension force ( $g$ , gravity acceleration;  $\rho$ , density of the droplet). According to the value of  $\text{Bo}$ , we divide the wetting phenomena into three categories. (I)  $\text{Bo} \ll 1$ . The droplet has a spherical cap with a cap radius  $R$ , see Fig. 1(b)(i). The distance of the droplet–air interface to the substrate is denoted by  $h(x)$ , where  $x$  is the radial coordinate in the cylindrical coordinate. We consider both sessile and pendant states in the case I. (II)  $\text{Bo} \gg 1$ . The droplet forms a pancake shape [26,27], whose thickness  $h(x)$  is nearly constant, see Fig. 1(b)(ii). We only consider the sessile state in the case II, since the pendant droplet may detach from the solid surface due to strong gravity effect. (III)  $\text{Bo} \sim 1$ . The droplet is depicted by an ellipsoidal cap, which has been well confirmed by experiments and numerical integrations [28–30]. The semi-axes of the ellipsoid is  $R/\sqrt{\alpha}$  and  $\alpha R$ , see Fig. 1(b)(iii);  $\alpha$  is a geometrical parameter measuring the deviation of the droplet shape from a spherical cap with  $\alpha = 1$ . The parameter  $R$  denotes the radius of an imaginary spherical cap (red dashed line) with the same volume as the ellipsoidal cap; the apex height of the imaginary spherical cap is  $(1 - \cos \theta_c)R$ . We consider both sessile ( $\alpha < 1$ ) and pendant ( $\alpha > 1$ ) states in the case III.

In all these three cases, the droplet shape is axisymmetric. The total free energy  $E$  of the system and the volume  $V$  of the droplet can be written as

$$E = \int_0^r \{2\pi x[\sigma(1 + h'^2)^{\frac{1}{2}} - \Delta\gamma] + u + l\} dx; \quad (1)$$

$$V = \int_0^r 2\pi x h(x) dx = \text{const}. \quad (2)$$

Here, we define  $\Delta\gamma = \gamma_{SG} - \gamma_{SL}$  and the integrand for  $E$  as  $E = \int_0^r e(h, h', x) dx$ ;  $h' = dh/dx$ . The first term in Eq. (1) depicts the energy contribution from the droplet cap and the base area. The  $u$ -term accounts for the bulk gravity effect with the energy density  $u = \pi x \rho g h^2 / 2$ . The  $l$ -term is expressed as  $l = 2\pi \lambda x h$  with the Lagrange multiplier  $\lambda$  arising from the volume constraint. According to the Bormashenko theory [31,32] (see also Blokhuis *et al.* [33] and Ref. [34]), the minimization of  $E$  is equivalent to the so-called transversality condition (TC) at the end point  $x = r$ , leading to Young's law with the equilibrium contact angle  $\theta_0$ , namely,

$$\text{TC: } (e - h' \partial e / \partial h')_{x=r} = 0 \Rightarrow \sigma \cos \theta_0 = \Delta\gamma. \quad (3)$$

Suffice to say, the bulk gravity effect does not affect the formulation of Young's law. However, the gravity does affect the solid–liquid interfacial energy, as will be addressed in the following.

In the case I, the volume  $V$  and the surface area  $S_c$  of the spherical cap have a closed form,  $V = \pi R^3 (1 - \cos \theta)^2 (2 + \cos \theta) / 3$  and  $S_c = 2\pi R^2 (1 - \cos \theta)$ . By using Eq. (3), we obtain the total free energy of the system as [10,37] (see Appendix)

$$\frac{E_I}{\sigma(3V\sqrt{\pi})^{\frac{2}{3}}} = \left(2 + \frac{\Delta\gamma}{\sigma}\right)^{\frac{1}{3}} \left(1 - \frac{\Delta\gamma}{\sigma}\right)^{\frac{2}{3}}. \quad (4)$$

In the case II, the total free energy is expressed as a function of the pancake thickness  $h$  as  $E_{II} = \pi r^2 (\sigma - \Delta\gamma) + \frac{1}{2} \rho g V h$ . By using the derivative  $\partial E_{II} / \partial h = 0$  to address the energy minimum and the condition  $\pi r^2 h \approx V$ , we obtain the total free energy as

$$E_{II} = \pi R_0^2 \frac{2\sqrt{\text{Bo}}}{3 \sin(\theta_0/2)} (\sigma - \Delta\gamma) + \frac{\rho g V R_0}{\sqrt{\text{Bo}}} \sin(\theta_0/2). \quad (5)$$

Here,  $\theta_0$  depends on  $\Delta\gamma$  for a fixed surface tension  $\sigma$ , as given by Eq. (3).

In the case III, with the closed form for the volume and the surface area of an ellipsoidal cap, we obtain the total free energy consisting of the droplet cap surface energy, fluids-solid surface energy, and droplet bulk gravity energy as

$$\frac{E_{III}}{\sigma \pi R^2} = \frac{1}{\alpha} \left[ 1 - f(\alpha) \cos \theta_0 + \nu(\alpha) - \sin^2 \theta_0 \frac{\Delta\gamma}{\sigma} \right] + \frac{\alpha \text{Bo}^2}{12} (1 - \cos \theta_0)^3 (3 + \cos \theta_0). \quad (6)$$

The two functions  $f(\alpha)$  and  $\nu(\alpha)$  only depend on the geometrical parameter  $\alpha$ , as given in the Appendix;  $\alpha$  has to be found numerically via  $\partial_\alpha E_{\text{III}} = 0$ .

When the volume  $V$ , surface tension  $\sigma$ , and density  $\rho$  are fixed, the total free energy  $E_{\text{I}}$ ,  $E_{\text{II}}$ , and  $E_{\text{III}}$  solely depends on  $\Delta\gamma$ . In contrast to the assumption of constant solid–liquid and solid–gas interfacial energies, we consider a composition-dependent  $\Delta\gamma$ . The physical origin for this consideration is a partial penetration of the fluid into the solid with a depth  $\ell$  [Fig. 1(a)(ii)]. This concept is consistent with Butt’s adaptation theory [38] and Tadmor’s experimental suggestion [39]. At the solid–fluid interface, we have nothing but a mixture of liquid and gas components. In such a consideration, the free energy density consists of internal energy, van der Waals interaction, and entropy of liquid–gas mixture as

$$\gamma = \ell[c + p + \chi_{\text{LG}}\phi(1 - \phi) + \chi_{\text{SG}}(1 - \phi) + \chi_{\text{SL}}\phi - Ts], \quad (7)$$

where  $\phi$  is the volume fraction of liquid species. According to Eq. (7), we have the following definition of the interfacial energies:

$$\gamma_{\text{SL}} = \gamma(\phi_{\text{L}}); \quad \gamma_{\text{SG}} = \gamma(\phi_{\text{G}}), \quad (8)$$

where  $\phi_{\text{L}}$  and  $\phi_{\text{G}}$  stand for the volume fraction of liquid species in the droplet and in the gas surrounding, respectively [40]. The equilibrium values of  $\phi_{\text{L}}$  and  $\phi_{\text{G}}$  are obtained by minimizing the total free energy, which will be discussed in Fig. 3.

The first part in Eq. (7) is the internal energy which is interpolated over the individual internal energy as  $\epsilon = \epsilon_{\text{L}}\phi + \epsilon_{\text{G}}(1 - \phi)$  ( $\epsilon_{\text{L}}$ , internal energy of liquid;  $\epsilon_{\text{G}}$ , internal energy of gas). The second term in Eq. (7) depicts the pressure; according to Dalton’s law, the static pressure is expressed as  $p = p_{\text{L}}\phi + p_{\text{G}}(1 - \phi)$ . Here, we consider the pressure of 1 atm for the gas ( $p_{\text{G}} = 1$  bar). The pressure of the liquid phase consists of both enthalpy and entropy contributions [45,46]. The latter one has been recently estimated to account for the line tension effect in polymer solutions [47]. However, the explicit form of the enthalpy and entropy contributions to the pressure is generally challenging to be formulated based on its physical origin, but can be equivalently calculated by the Young-Laplace equation as

$$\text{I: } p_{\text{L}} = p_{\text{G}} + \frac{2\sigma}{R}, \quad \text{Bo} \ll 1; \quad (9)$$

$$\text{II: } p_{\text{L}} = p_{\text{G}} + \frac{\rho g V}{\eta \pi r^2}, \quad \text{Bo} \gg 1; \quad (10)$$

$$\text{III: } p_{\text{L}} = p_{\text{G}} + \sigma \left( \frac{1}{R_1} + \frac{1}{R_2} \right) \pm \frac{\rho g V}{\eta \pi r^2}, \quad \text{Bo} \sim 1. \quad (11)$$

The parameters  $R_1$  and  $R_2$  in Eq. (11) stand for the principal radii of the ellipsoid at the contact line;  $\eta \geq 1$  accounts for the macroscopic roughness that modifies the effective

contact area between liquid and solid. Unless otherwise stated, we set  $\eta = 1$  in the following discussion for brevity. By choosing a reference plane  $z = 0$  on the solid surface, the “+” and “−” signs in Eq. (11) correspond to sessile and pendant droplets, respectively.

The third, fourth, and fifth terms in Eq. (7) account for the van der Waals interaction of liquid–gas, gas–solid, and liquid–solid, respectively, similar to the consideration in the Flory-Huggins theory [48–50]. The intermolecular potential of liquid–gas, gas–solid, and liquid–solid is depicted by  $\chi_{\text{LG}}$ ,  $\chi_{\text{SG}}$ , and  $\chi_{\text{SL}}$ , respectively [37], which can be quantified by experiments [51,52] or molecular theory models [53]. The last term in Eq. (7) describes the entropy contribution with entropy density  $s$  and temperature  $T$  [54]. Considering all these contributions, we express the difference of the gas–solid and liquid–solid interfacial energies as

$$\text{I: } \Delta\gamma = \Delta\gamma_0 + 2\ell\Delta\phi\sigma/R; \quad (12)$$

$$\text{II: } \Delta\gamma = \Delta\gamma_0 + \ell\Delta\phi\rho g V/\pi r^2; \quad (13)$$

$$\text{III: } \Delta\gamma = \Delta\gamma_0 + \ell\Delta\phi \left[ \sigma \left( \frac{1}{R_1} + \frac{1}{R_2} \right) \pm \frac{\rho g V}{\pi r^2} \right], \quad (14)$$

where  $\Delta\phi$  is defined as  $\Delta\phi = (\phi_{\text{G}} - \phi_{\text{L}})$ . The interfacial energy difference  $\Delta\gamma_0$  corresponds to the rest terms except the pressure for the difference in the internal energy and the van der Waals force, as discussed in our previous work [37]. The last term depicts the contribution of the pressure, which is the most central consideration of the current Letter. In comparison with the definition for the line tension  $\tau$  according to  $\sigma \cos \theta = \sigma \cos \theta_0 + \tau/r$  [23], we obtain the line energy as

$$\text{I: } \tau_1 = 2\ell\Delta\phi\sigma \sin \theta_0, \quad \text{Bo} \ll 1; \quad (15)$$

$$\text{II: } \tau_2 = \ell\Delta\phi\rho g V/(\pi r), \quad \text{Bo} \gg 1; \quad (16)$$

$$\text{III: } \tau_3^\pm = \ell\Delta\phi \left[ r\sigma \left( \frac{1}{R_1} + \frac{1}{R_2} \right) \pm \frac{\rho g V}{\pi r} \right], \quad \text{Bo} \sim 1. \quad (17)$$

From the above equations (15)–(17), we see two important conclusions: (i) The magnitude of the line energy is controlled by  $\ell\sigma$  as well as  $\ell\rho g V/(\pi r)$ . (ii) The sign of the line energy is manipulated by two factors:  $\Delta\phi$ , which will be discussed later, and pendant or sessile states (see Appendix). For sessile droplets, when  $\Delta\phi > 0$ , we have the positive line energy; when  $\Delta\phi < 0$ , we have the negative line energy.

Note that the surface tension  $\sigma$  in the above equations can have a strong dependence on the droplet size for nanoscaled droplets, known as the Tolman effect [15], which results in an additional line tension effect; this discussion has been presented in Refs. [14,17,20].

In the case III, we evaluate the mean curvature of the ellipsoidal cap at the contact line and obtain the line energy as

$$\tau_3^\pm = \ell \left[ 2\sigma\varphi_1 \pm \frac{1}{3}\rho g r^2 \frac{2 + \cos\theta_0}{(1 + \cos\theta_0)^2} \varphi_2 \right] \Delta\phi \sin\theta_0. \quad (18)$$

Here, the two factors  $\varphi_1$  and  $\varphi_2$  are expressed as

$$\varphi_1 = \frac{2 + (\alpha^{-3} - 1)(1 + \cos^2\theta_0)}{2[\alpha^{-3}\cos^2\theta_0 + \sin^2\theta_0]^{\frac{3}{2}}}; \quad \varphi_2 = \alpha^{\frac{3}{2}}. \quad (19)$$

When  $\alpha = 1$  corresponding to a spherical cap, both factors  $\varphi_1$  and  $\varphi_2$  are equal to 1.

Figure 2(a) depicts the line energy  $\tau_3^+$  of sessile water droplets as a function of the base radius  $r$ . Parameters are  $\sigma = 0.072$  N/m,  $g = 9.81$  m/s<sup>2</sup>,  $\rho = 1000$  kg/m<sup>3</sup>,  $\Delta\phi = 1$ , and  $\ell = 10$  nm. The red solid line depicts the line energy for the spherical cap model by setting  $\alpha = 1$  in Eq. (18), while the red triangle symbols describe the line energy for an ellipsoidal cap, both for  $\theta_0 = 30^\circ$ . In the ellipsoidal model,  $\alpha$  in the coefficients  $\varphi_1$  and  $\varphi_2$  is obtained numerically via solving  $\partial_\alpha E_{\text{III}} = 0$ . In both models, the line energy ranges from 0.5 to about 100 nN. The results between spherical and ellipsoidal caps overlap when the base radius is less than about 0.01 m. In this case, the line energy  $\tau_3^+$  converges to a constant value, as given by  $\tau_1$ ; it is sufficient to use Eq. (15) to calculate the line energy. When the base radius is greater than 0.01 m, the difference between the spherical cap model and the ellipsoidal cap model increases with  $r$ . For other Young's contact angles,  $\theta_0 = 60^\circ, 120^\circ$ , similar results are observed; for a fixed droplet size, an increase in the Young's contact angle  $\theta_0$  leads to an increase in the line energy. For comparison, the line energy of the pancake model  $\tau_2$  is illustrated by the dot-dot-dashed line in Fig. 2(a). The ellipsoidal model is nearly the same as the pancake model for relatively large base radius.

Figures 2(b) and 2(c) present a quantitative comparison of  $\tau_1$  versus  $T - T_c$  with experiments [41] and existing theories (Ising model,  $\tau^{\text{Ising}}$ ; Indekeu model,  $\tau^{\text{I}}$ ; Joanny-de Gennes model,  $\tau^{\text{J}}$ , see Appendix) near the critical temperature  $T_c$  for continuous wetting. For the positive line tension, we set  $\Delta\phi = 1$ ;  $\tau_1$  decays to zero until the critical temperature (red line), showing a good agreement with experiments (triangle). For the negative line tension [Fig. 2(c)], we set  $\Delta\phi = -1$ ;  $\tau_1$  exhibits a good consistency with Indekeu theory  $\tau^{\text{I}}$  [42,43] as well as with Joanny-de Gennes model, and Ising model, the same via  $\tau_0 = \sigma_0\ell = 1$  pN. Note that our result has an additional factor  $\sin\theta_0$ . This can be used to explain the vanishing line tension at the first order wetting transition temperature  $T_w$ , where the contact angle becomes zero, being consistent

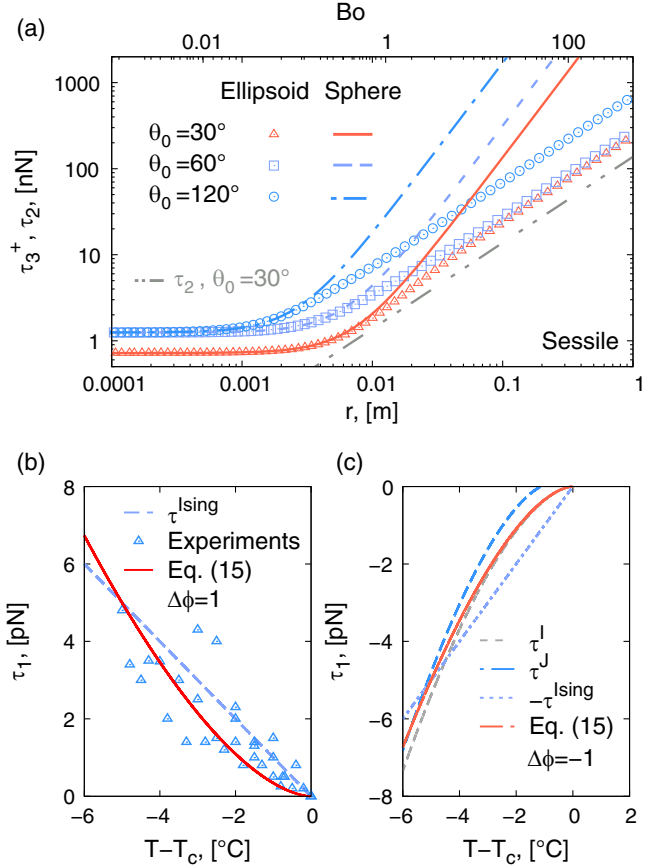


FIG. 2. (a) The line energy  $\tau_3^+$  [Eq. (18)] and  $\tau_2$  [Eq. (16)] for sessile water droplets versus the base radius  $r$  for different Young's contact angles  $\theta_0$ . Lines, the spherical cap model with  $\alpha = 1$ ; symbols, the ellipsoidal cap model with  $\alpha < 1$ . The Bond number,  $Bo$  for  $\theta_0 = 30^\circ$  is shown in the top axis. (b) Comparison of  $\tau_1$  according to Eq. (15) with experiments [41] and Ising model  $\tau^{\text{Ising}}$ . (c) Comparison of  $\tau_1$  with Ising model  $-\tau^{\text{Ising}}$ , Indekeu theory  $\tau^{\text{I}}$  [42,43], and Joanny-de Gennes theory  $\tau^{\text{J}}$  [44].

with the conclusion of Starov and co-workers [57] and Widom and Clark [58]. The factor  $\sin\theta_0$  can also explain the counterintuitive result that sometimes the line tension increases with temperature [59], since  $\theta_0$  can increase with temperature [60].

Next, we address the sign of  $\Delta\phi$  by deriving the expression for the equilibrium compositions of liquid beneath the droplet  $\phi_L^e$  and in the gas  $\phi_G^e$ . We assume that the equilibrium compositions  $\phi_L^e$  and  $\phi_G^e$  are not significantly affected by the pressure [61]. In the case I, substituting  $\Delta\gamma_0$  into Eq. (4) and minimizing the total free energy  $E_1(\phi_L, \phi_G)$  subjected to the constraint  $0 \leq \phi_L \leq 1$  and  $0 \leq \phi_G \leq 1$  for constant  $V$  and  $\sigma$ , we obtain two sets of equilibrium composition of  $\phi_L^e$  and  $\phi_G^e$  as

$$\text{micro-Cassie: } \phi_G^e = \frac{1}{2} \left( 1 - \frac{\Delta\epsilon - \Delta\chi}{\chi_{\text{LG}}} \right), \quad \phi_L^e = 0; \quad (20)$$

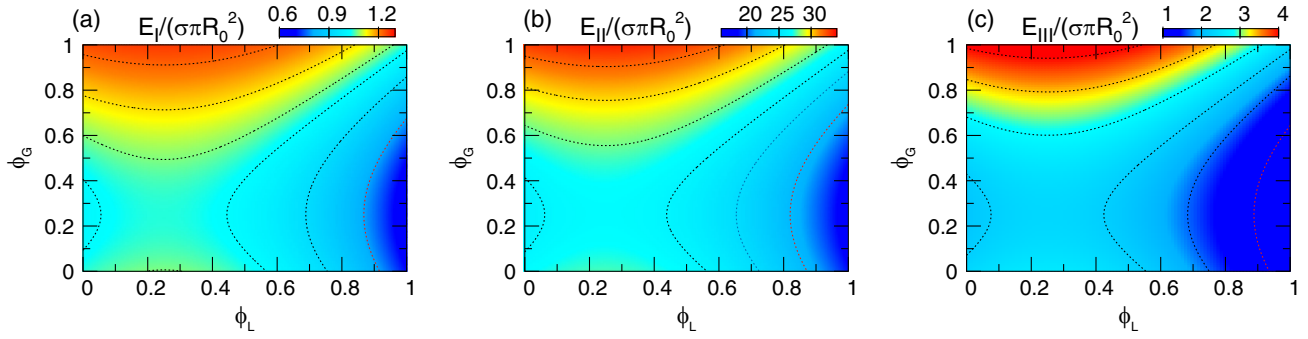


FIG. 3. (a) Energy map  $E_I(\phi_L, \phi_G)$  for  $(\Delta\epsilon - \Delta\chi)/\chi_{LG} = 0.5$  and  $Bo = 0.1$ . (b) Energy map  $E_{II}(\phi_L, \phi_G)$  for  $Bo = 100$ . (c) Energy map  $E_{III}(\phi_L, \phi_G)$  for  $Bo = 1$ ; for each pair of  $\phi_L$  and  $\phi_G$ , the geometrical parameter  $\alpha$  is obtained via solving  $\partial_\alpha E_{III} = 0$ . Two local minima are observed in all energy maps. The left minimum  $\phi_L^e = 0$  is the micro-Cassie state and the right minimum  $\phi_L^e = 1$  is the micro-Wenzel state, as quantified in Eqs. (20) and (21).

$$\text{micro-Wenzel: } \phi_G^e = \frac{1}{2} \left( 1 - \frac{\Delta\epsilon - \Delta\chi}{\chi_{LG}} \right), \quad \phi_L^e = 1, \quad (21)$$

where  $\Delta\epsilon = \epsilon_G - \epsilon_L$  denotes the difference in the internal energy of gas and liquid, and  $\Delta\chi = \chi_{SL} - \chi_{SG}$  represents the difference in the van der Waals force of solid–gas and solid–liquid. Differentiating by the equilibrium composition of the liquid in the solid beneath the droplet, we call these two states in Eqs. (20) and (21) as micro-Cassie and micro-Wenzel states, respectively. In the micro-Cassie state, the liquid composition in the solid is 0; in the micro-Wenzel state, the liquid composition in the solid phase is 1. Based on Eqs. (20) and (21), we address the sign of the line tension according to  $\Delta\phi = \phi_G - \phi_L$  for sessile droplets as

$$\text{positive line tension: } \Delta\phi = \phi_G^e > 0; \quad (22)$$

$$\text{negative line tension: } \Delta\phi = \phi_G^e - 1 < 0. \quad (23)$$

An example of the energy map  $E_I(\phi_L, \phi_G)$  is shown in Fig. 3(a) for  $(\Delta\epsilon - \Delta\chi)/\chi_{LG} = 0.5$ . Two local minima are observed in the energy map:  $(\phi_L^e, \phi_G^e) = (0, 0.25)$  (left minimum) and  $(\phi_L^e, \phi_G^e) = (1, 0.25)$  (right minimum), which are well consistent with Eqs. (20) and (21).

In the cases II and III, the energy maps are illustrated in Figs. 3(b) and 3(c), respectively. Here, we set a Bond number of 100 in the case II and a Bond number of 1 in the case III. As demonstrated by the energy maps in both cases, the position of the energy minimum is almost not affected; only the magnitude of the total energy is modified (see the color legend).

In conclusion, we have proposed an alternative concept quantifying the gravity effect on the line tension; for the first time, to the best knowledge of the authors, we derive the line energy in terms of physical parameters. Our finding can be used to explain previous experimental data of line energy spanning from  $1 \times 10^{-11}$  to  $1 \times 10^{-6}$  N, shedding light on the controversial issue of gravity effect on the wetting phenomena. Moreover, we address that the sign of

the line energy is controlled by two key factors: micro-Cassie or micro-Wenzel states, sessile or pendant states.

*Acknowledgments*—We thank the referee for deriving all equations presented in first version of the Letter and pointing out that some factors are missing in our derivation. This research is supported by VirtMat project ‘‘VirtMat P09: Wetting Phenomena’’ of the Helmholtz association, as part of the program ‘‘MSE-materials science and engineering’’ No. 43.31.01. H. Z. is thankful for funding of the research through the Gottfried-Wilhelm Leibniz prize NE 822/31-1 of the German Research Foundation (DFG).

- 
- [1] A. Marmur, *Langmuir* **20**, 3517 (2004).
  - [2] E. Y. Bormashenko, *Wetting of Real Surfaces* (Walter de Gruyter GmbH & Co KG, Leipzig, 2018), Vol. 19.
  - [3] P.-G. De Gennes, *Rev. Mod. Phys.* **57**, 827 (1985).
  - [4] F. Wang, Y. Wu, and B. Nestler, *Adv. Mater.* **35**, 2210745 (2023).
  - [5] E. Bormashenko, *Adv. Colloid Interface Sci.* **222**, 92 (2015).
  - [6] T. Young, *Phil. Trans. R. Soc. London* **95**, 65 (1805).
  - [7] A. Amirfazli and A. Neumann, *Adv. Colloid Interface Sci.* **110**, 121 (2004).
  - [8] R. Tadmor, *Surf. Sci.* **602**, L108 (2008).
  - [9] R. Tadmor, *Langmuir* **37**, 6357 (2021).
  - [10] G. Whyman, E. Bormashenko, and T. Stein, *Chem. Phys. Lett.* **450**, 355 (2008).
  - [11] P.-G. Gennes, F. Brochard-Wyart, D. Quéré *et al.*, *Capillarity and Wetting Phenomena: Drops, Bubbles, Pearls, Waves* (Springer, New York, 2004).
  - [12] J. K. Berg, C. M. Weber, and H. Riegler, *Phys. Rev. Lett.* **105**, 076103 (2010).
  - [13] M. A. Anisimov, *Phys. Rev. Lett.* **98**, 035702 (2007).
  - [14] M. Lulli, L. Biferale, G. Falcucci, M. Sbragaglia, and X. Shan, *Phys. Rev. E* **105**, 015301 (2022).
  - [15] R. C. Tolman, *J. Chem. Phys.* **17**, 333 (1949).
  - [16] Y. A. Lei, T. Bykov, S. Yoo, and X. C. Zeng, *J. Am. Chem. Soc.* **127**, 15346 (2005).
  - [17] B. H. Tan, H. An, and C.-D. Ohl, *Phys. Rev. Lett.* **130**, 064003 (2023).

- [18] R. E. Johnson Jr., *J. Phys. Chem.* **63**, 1655 (1959).
- [19] F. Wang, H. Zhang, Y. Wu, and B. Nestler, *J. Fluid Mech.* **970**, A17 (2023).
- [20] H. Zhang, Y. Wu, F. Wang, and B. Nestler, *J. Chem. Phys.* **159**, 164701 (2023).
- [21] F. Wang and B. Nestler, *J. Chem. Phys.* **154**, 094704 (2021).
- [22] B. Widom, *J. Phys. Chem.* **99**, 2803 (1995).
- [23] L. Schimmele, M. Napiórkowski, and S. Dietrich, *J. Chem. Phys.* **127**, 164715 (2007).
- [24] T. Zhao and L. Jiang, *Colloids Surf. B* **161**, 324 (2018).
- [25] A. W. Neumann, R. David, and Y. Zuo, *Applied Surface Thermodynamics* (CRC Press, New York, 2010), Vol. 151.
- [26] H. E. Huppert, *J. Fluid Mech.* **121**, 43 (1982).
- [27] L. Hocking, *Q. J. Mech. Appl. Math.* **36**, 55 (1983).
- [28] G. Whyman and E. Bormashenko, *J. Colloid Interface Sci.* **331**, 174 (2009).
- [29] V. A. Lubarda and K. A. Talke, *Langmuir* **27**, 10705 (2011).
- [30] Y. Yu, C. Lv, L. Wang, and P. Li, *ACS Omega* **5**, 26732 (2020).
- [31] E. Bormashenko, *Colloids Surf. A* **345**, 163 (2009).
- [32] E. Bormashenko, *J. Adhes. Sci. Technol.* **34**, 219 (2020).
- [33] E. Blokhuis, Y. Shilkrot, and B. Widom, *Mol. Phys.* **86**, 891 (1995).
- [34] See Supplemental Material at <http://link.aps.org/supplemental/10.1103/PhysRevLett.133.246201> for the derivation, which includes Refs. [35–36].
- [35] I. M. Gelfand, R. A. Silverman *et al.*, *Calculus of Variations* (Courier Corporation, New Jersey, 2000).
- [36] B. Shapiro, H. Moon, R. L. Garrell, and C.-J. C. Kim, *J. Appl. Phys.* **93**, 5794 (2003).
- [37] F. Wang and B. Nestler, *Phys. Rev. Lett.* **132**, 126202 (2024).
- [38] H.-J. Butt, R. Berger, W. Steffen, D. Vollmer, and S. A. Weber, *Langmuir* **34**, 11292 (2018).
- [39] R. Tadmor, P. Bahadur, A. Leh, H. E. N'guessan, R. Jaini, and L. Dang, *Phys. Rev. Lett.* **103**, 266101 (2009).
- [40] The volume fraction of gas species in the droplet and in the surrounding at the solid surface is  $1 - \phi_L$  and  $1 - \phi_G$ , respectively.
- [41] A. R. Honerkamp-Smith, P. Cicuta, M. D. Collins, S. L. Veatch, M. Den Nijs, M. Schick, and S. L. Keller, *Biophys. J.* **95**, 236 (2008).
- [42] J. Indekeu, *Int. J. Mod. Phys. B* **08**, 309 (1994).
- [43] J. Indekeu, *Physica (Amsterdam)* **183A**, 439 (1992).
- [44] J. Joanny and P. De Gennes, *J. Colloid Interface Sci.* **111**, 94 (1986).
- [45] According to the Landau potential, the pressure may be defined as  $-p = f - \mu\phi$  [19,46], where the free energy density  $f$  and the associated chemical potential  $\mu$  consist of both enthalpy and entropy contributions.
- [46] R. Borcia and M. Bestehorn, *Phys. Rev. E* **75**, 056309 (2007).
- [47] E. Bormashenko, *Entropy* **20**, 712 (2018).
- [48] P. J. Flory, *J. Chem. Phys.* **10**, 51 (1942).
- [49] M. L. Huggins, *J. Chem. Phys.* **9**, 440 (1941).
- [50] F. Wang, P. Altschuh, L. Ratke, H. Zhang, M. Selzer, and B. Nestler, *Adv. Mater.* **31**, 1806733 (2019).
- [51] H.-J. Butt, *Biophys. J.* **60**, 1438 (1991).
- [52] A. Kundu, S. Paul, S. Banerjee, and A. Banerjee, *Appl. Phys. Lett.* **115**, 123701 (2019).
- [53] W. Zhang, E. D. Gomez, and S. T. Milner, *Phys. Rev. Lett.* **119**, 017801 (2017).
- [54] The Boltzmann mixing entropy is expressed as  $\gamma_s(\phi) = -\ell T s = \ell k_b T [\phi \ln \phi + (1 - \phi) \ln(1 - \phi)]$  ( $k_b$ , Boltzmann constant), which has the shape of a parabola opening upward and may be approximated as  $\gamma_s \approx a(\phi - \frac{1}{2})^2 + b$  ( $a$  and  $b$  are temperature-dependent constants). The rest term excluding  $p$  in  $\gamma(\phi)$  is a second order polynomial of  $\phi$ , so that the  $\gamma_s$  term only modifies the coefficients of the parabola of  $\gamma(\phi)$ . As shown in [37], a parabolic wall free energy with varying coefficients always leads to two local minima of  $E_I$ , one at  $\phi_L^e = 0$ ,  $\phi_G^e = f(X)$  and the other one at  $\phi_L^e = 1$ ,  $\phi_G^e = f(X)$ , where  $f$  is a function of  $X = \{\epsilon_G, \epsilon_L, \chi_{LG}, \chi_{SG}, \chi_{SL}\}$ . By adding the new entropy term  $\gamma_s$ , the energy landscape remains, since it is also a parabola of  $\phi$  but with modified coefficients. By considering  $\gamma_s$ , the energy minima are at  $\phi_L^e = 0$ ,  $\phi_G^e = f(a, b, X)$  and  $\phi_L^e = 1$ ,  $\phi_G^e = f(a, b, X)$ . When higher order terms  $\phi^4, \phi^6, \dots$  are considered in  $\gamma_s$ , it becomes hard to have a closed form for the equilibrium composition.
- [55] J. W. Cahn, *J. Chem. Phys.* **66**, 3667 (1977).
- [56] In Ref. [55], the factor is 1.3; in Ref. [42], the factor is 1.26. The change of the factor leads to a very minor modification to the comparison.
- [57] N. V. Churaev, V. Starov, and B. Derjaguin, *J. Colloid Interface Sci.* **89**, 16 (1982).
- [58] B. Widom and A. Clarke, *Physica (Amsterdam)* **168A**, 149 (1990).
- [59] A. J. García-Sáez, S. Chiantia, and P. Schwille, *J. Biol. Chem.* **282**, 33537 (2007).
- [60] J.-W. Song and L.-W. Fan, *Adv. Colloid Interface Sci.* **288**, 102339 (2021).
- [61] If the composition or density distribution is affected by the gravity effect, we refer to a recent work of Tan *et al.* [17] and the classic Cahn–de Gennes theory [3,55].

## End Matter

*Appendix*—Derivation of the total free energy, effect of pendant and sessile states, and existing theories for line tension.

Case I: Spherical cap The volume  $V$  and the surface  $S_c$  of a spherical cap with a radius  $R$  read

$$V = \frac{\pi R^3}{3}(1 - \cos\theta)^2(2 + \cos\theta); \quad S_c = 2\pi R^2(1 - \cos\theta).$$

The total interfacial energy of the system reads

$$E_I = \sigma S_c + \Delta\gamma\pi R^2 \sin^2\theta + \gamma_{SG}\Gamma,$$

in which the last term is scaled by the total surface area of the solid surface  $\Gamma$  and is considered as a reference value. Neglecting the reference value  $\Gamma\gamma_{SG}$ , we obtain the total free energy as

$$E_I = \varepsilon(1 - \cos\theta)(2 + \cos\theta)[2\sigma - \Delta\gamma(1 + \cos\theta)],$$

with the factor  $\varepsilon = (9\pi V^2)^{1/3}/[(1 - \cos\theta)^{\frac{4}{3}}(2 + \cos\theta)^{\frac{5}{3}}]$ . Next, we differentiate  $E_I$  to  $\theta$ , yielding

$$\frac{dE_I}{d\theta} = \left[ \frac{9\pi V^2}{(1 - \cos\theta)^4 (2 + \cos\theta)^5} \right]^{\frac{1}{3}} 2(\Delta\gamma - \sigma \cos\theta) \sin\theta.$$

The solution of  $dE_I/d\theta = 0$  gives rise to Young's equation:  $\Delta\gamma = \sigma \cos\theta_0$ . Substituting the Young's equation into the above equation for  $E_I$ , we obtain Eq. (4).

**Case II: Pancake shape** At very strong gravity impact, the droplet is drastically deformed into a pancake shape, as illustrated in Fig. 1(b)(ii). In this case, the droplet volume  $V \approx \pi r^2 h$  is associated with the pancake height  $h$  and the base radius  $r$ . The total free energy can be written as

$$E_{II} = \pi r^2 (\sigma - \Delta\gamma) + \frac{1}{2} \rho g V h.$$

The first term denotes the total surface energy, while the last term stands for the bulk gravitational energy. The equilibrium droplet shape is addressed via  $\partial E_{II}/\partial h = 0$ , which leads to

$$h = 2R_0 \sin(\theta_0/2) / \sqrt{\text{Bo}};$$

$$r = \sqrt{\frac{2}{3}} R_0 \text{Bo}^{\frac{1}{4}} / \sqrt{\sin(\theta_0/2)}.$$

Thus, the total free energy  $E_{II}$  is expressed by Eq. (5).

**Case III: Ellipsoidal cap** Considering the gravity effect on the formation of an oblate ellipsoidal cap, we write the ellipsoidal contour with the following parametric equation as

$$\alpha^3 x^2 + (z - \alpha R)^2 = \alpha^2 R^2.$$

Here, two hemiaxes are scaled by  $R/\sqrt{\alpha}$  and  $\alpha R$ , as depicted in Fig. 1(b)(iii);  $R$  is the radius of an imaginary spherical cap with the same volume. The volume  $V$  of the ellipsoidal cap by using the parametric equation and upon integration is expressed as

$$V = \frac{\pi R^3}{3} (1 - \cos\theta_0)^2 (2 + \cos\theta_0).$$

At equilibrium, we assume  $\theta_c \approx \theta_0$  (see Fig. 1). The surface area of the whole ellipsoid according to the integration  $S = 2 \int_0^{R/\sqrt{\alpha}} a dx$ , where  $a = 2\pi x \sqrt{1 + (h')^2}$  is written as

$$S = \frac{2\pi R^2}{\alpha} \left( 1 + \frac{\alpha^3}{2k} \ln \frac{1+k}{1-k} \right), \quad k = \sqrt{1 - \alpha^3}.$$

The surface area of the ellipsoidal cap  $S_c$  is obtained by subtracting  $S'$  from  $S$ ;  $S' = \int_0^{R \sin\theta_0/\sqrt{\alpha}} a dx$  denotes the surface area of the ellipsoid truncated by the substrate. Hence, the surface area of the ellipsoidal cap reads

$$S_c = S - S' = \frac{\pi R^2}{\alpha} [1 - f(\alpha) \cos\theta_0 + \nu(\alpha)],$$

where we have defined two functions  $f(\alpha)$  and  $\nu(\alpha)$  as  $\nu(\alpha) = (\alpha^3/k) \ln\{-k \cos\theta_0 + f(\alpha)\}/(1-k)$ ;  $f(\alpha) = \sqrt{1 - k^2 \sin^2\theta_0}$ . The contact area of the droplet with the solid substrate is formulated as  $S_b = \pi R^2 \sin^2\theta_0/\alpha$ . Thus, the total surface energy of the droplet reads

$$\frac{E_s}{\sigma \pi R^2} = \frac{1}{\alpha} \left[ 1 - f(\alpha) \cos\theta_0 + \nu(\alpha) - \sin^2\theta_0 \frac{\Delta\gamma}{\sigma} \right].$$

The bulk gravity energy of the droplet with the height of the centroid  $\bar{z}$  is expressed as

$$E_g = \rho g V \bar{z} = \frac{\alpha \rho g \pi R^4}{12} (1 - \cos\theta_0)^3 (3 + \cos\theta_0),$$

so that the total energy of the whole droplet including surface and bulk gravity energies reads  $E_{III} = E_s + E_g$ , leading to Eq. (6).

**Existing theories** For  $\text{Bo} \ll 1$ , the line tension versus temperature according to Ising model  $\tau^{\text{Ising}}$ , Indekeu theory  $\tau^I$  [42,43], and Joanny-de Gennes theory  $\tau^J$  [44] reads

$$\tau^{\text{Ising}} = \tau_0 (T - T_c);$$

$$\tau^I = -\ell \sigma \theta_0 = -\tau_0 (T - T_c)^{1.3} \theta_0;$$

$$\tau^J = -\ell \sigma (\ln\theta_0 + 1) = -\tau_0 (T - T_c)^{1.3} (\ln\theta_0 + 1).$$

**Effect of pendant and sessile states** For the pendant state, a negative sign occurs in the second term in Eq. (18). The competing effect of surface tension with gravity leads to a variation in the sign of the line tension. The critical base radius  $r_c$  for the sign transition is

$$r_c = \sqrt{\frac{6\sigma\varphi_1}{\rho g \varphi_2}} (1 + \cos\theta_0) (2 + \cos\theta_0)^{-\frac{1}{2}}.$$

When the base radius is less than  $r_c$ , the surface tension related pressure dominates the gravity related pressure. For large radius droplets with  $r > r_c$ , the main contribution to the line energy is the gravity.